



12-1991

Reconstruction of a rocket motor time point image from limited projection data

Alan Paul Smith

Follow this and additional works at: https://trace.tennessee.edu/utk_gradthes

Recommended Citation

Smith, Alan Paul, "Reconstruction of a rocket motor time point image from limited projection data. " Master's Thesis, University of Tennessee, 1991.
https://trace.tennessee.edu/utk_gradthes/12538

This Thesis is brought to you for free and open access by the Graduate School at TRACE: Tennessee Research and Creative Exchange. It has been accepted for inclusion in Masters Theses by an authorized administrator of TRACE: Tennessee Research and Creative Exchange. For more information, please contact trace@utk.edu.

To the Graduate Council:

I am submitting herewith a thesis written by Alan Paul Smith entitled "Reconstruction of a rocket motor time point image from limited projection data." I have examined the final electronic copy of this thesis for form and content and recommend that it be accepted in partial fulfillment of the requirements for the degree of Master of Science, with a major in Electrical Engineering.

Bruce W. Bomar, Major Professor

We have read this thesis and recommend its acceptance:

Roy Joseph, Ron Belz

Accepted for the Council:

Carolyn R. Hodges

Vice Provost and Dean of the Graduate School

(Original signatures are on file with official student records.)


To the Graduate Council:

I am submitting herewith a thesis written by Alan Paul Smith, entitled "Reconstruction of a Rocket Motor Time Point Image from Limited Projection Data." I have examined the final copy of this thesis for form and content and recommend that it be accepted in partial fulfillment of the requirements for the degree of Master of Science, with a major in Electrical Engineering.



Bruce W. Bomar, Major Professor

We have read this thesis
and recommend its acceptance:



Accepted for the Council:



Vice Provost
and Dean of The Graduate School

STATEMENT OF PERMISSION TO USE

In presenting this thesis in partial fulfillment of the requirements for a Master's degree at the University of Tennessee, Knoxville, I agree that the library shall make it available to borrowers under rules of the library. Brief quotations from this thesis are allowable without special permission, provided that accurate acknowledgment of the source is made.

Permission for extensive quotation from or reproduction of this thesis may be granted by my major professor, or in his absence, by the Head of Interlibrary Services when, in the opinion of either, the proposed use of the material is for scholarly purposes. Any copying or use of the material in this thesis for financial gain shall not be allowed without my written permission.

Signature *W. P. Smith*

Date 11/25/91

RECONSTRUCTION OF A ROCKET MOTOR
TIME POINT IMAGE FROM LIMITED
PROJECTION DATA

A Thesis
Presented for the
Master of Science
Degree
The University of Tennessee, Knoxville

Alan Paul Smith
December 1991

ACKNOWLEDGMENTS

The author would like to express his appreciation to Dr. Bruce Bomar, who served as the chairman of the committee, and Dr. Roy Joseph, who served as a member of the committee, for their helpful advice and guidance.

A special thanks is due to Dr. Ron Belz for his encouragement and invaluable support and guidance in conducting this investigation. This thesis would not be realized without his help.

The author would also like to thank his parents for their support during this investigation.

ABSTRACT

A correction-reconstruction algorithm was developed to reconstruct a rocket motor time point image from a limited amount of projection data and known image information. Conjugate gradient optimization was used in the correction-reconstruction process. The known image information included geometry and density information about the rocket motor.

To test the algorithm, a priori information was used to reconstruct two rocket motor time point images, a pre-test image and a first time point image, from a limited number of simulated projection data sets. The pre-test image is the zero time point image of the rocket motor. The simulated projection data sets were free of noise and were computed by using model images of a solid-fuel rocket motor. The pre-test and first time point images were compared after reconstructing both images with and without the use of a priori information. Error function values were used to measure the quality of the reconstructed images. Both images were better, as shown by the error function values, when a priori information was used to reconstruct them. A termination criterion for the conjugate gradient reconstruction algorithm and the correction-reconstruction process was also developed.

TABLE OF CONTENTS

CHAPTER	PAGE
I. INTRODUCTION	1
II. BACKGROUND INFORMATION	5
1. TYPES OF PROJECTION DATA	5
<u>Object Projection Data</u>	5
<u>Image Projection Data</u>	6
2. CONJUGATE GRADIENT RECONSTRUCTION	
ALGORITHM	7
<u>Chi-Square Function</u>	8
<u>Iteration Scheme</u>	9
III. CORRECTION-RECONSTRUCTION PROCESS	11
1. CORRECTION OF KNOWN REGIONS	11
<u>Sources of A Priori Information</u>	11
<u>A Priori Information Parameters</u>	12
2. TERMINATION CRITERION	13
<u>Termination Values</u>	13
<u>Difference Function Data</u>	14
IV. RESULTS OF THE PROCESS	16
1. METHOD OF TESTING THE PROCESS	16
<u>Model Images</u>	16
<u>Use of Model Images</u>	17
2. RECONSTRUCTION OF THE IMAGES	18
<u>Pre-Test Image Reconstructions</u>	18
<u>First Time Point Image Reconstructions</u>	20

V. SUMMARY	24
1. DISCUSSION OF RESULTS	24
2. SUGGESTIONS FOR FUTURE WORK	25
BIBLIOGRAPHY	26
APPENDICES	29
VITA	49

LIST OF TABLES

TABLE	PAGE
4.1 Test Run Function Values for Conjugate Gradient Iterations of Pre-Test Image Reconstruction.	43
4.2 Test Run Function Values for Process Iterations of Pre-Test Image Reconstruction.	43
4.3 Error Function Values of Pre-Test Images Reconstructed from Different Numbers of Data Sets.	44
4.4 Test Run Function Values for Conjugate Gradient Iterations of First Time Point Image Reconstruction.	44
4.5 Test Run Function Values for Process Iterations of First Point Image Reconstruction.	45
4.6 Error Function Values of First Time Point Images Reconstructed from Different Numbers of Data Sets.	45

LIST OF FIGURES

FIGURE	PAGE
1.1 Data Acquisition Equipment.	28
1.2 Burnout of Propellant during Test.	28
2.1 Object Projection Path.	29
2.2 Parallel-Beam Data Acquisition.	29
2.3 Fan-Beam Data Acquisition.	30
2.4 Image Projection Paths.	30
2.5 Conjugate Gradient Reconstruction Algorithm.	31
3.1 Correction-Reconstruction Process.	32
3.2 Rocket Motor Time Point Image.	33
3.3 Known Regions of Estimate Image.	33
4.1 Model Pre-Test Image.	34
4.2 Model First Time Point Image.	34
4.3 Error Function Values for Conjugate Gradient Iterations of Pre-Test Image Reconstruction.	35
4.4 Pre-Test Image Reconstructed from 11 Conjugate Gradient Iterations(256 Grey Level Values).	35
4.5 Pre-Test Image Reconstructed from 11 Conjugate Gradient Iterations(4 Grey Level Values).	36
4.6 Error Function Values for Process Iterations of Pre-Test Image Reconstruction.	36
4.7 Pre-Test Image Reconstructed from 19 Process Iterations(4 Grey Level Values).	37
4.8 Error Function Values of Pre-Test Images Reconstructed from Different Numbers of Data Sets.	37
4.9 Error Function Values for Conjugate Gradient Iterations of First Time Point Image Reconstruction.	38

4.10	First Time Point Image Reconstructed from Four Conjugate Gradient Iterations(4 Grey Level Values).	38
4.11	Error Function Values for Process Iterations of First Time Point Image Reconstruction.	39
4.12	First Time Point Image Reconstructed from 11 Process Iterations(4 Grey Level Values).	39
4.13	Error Function Values of First Time Point Images Reconstructed from Different Numbers of Data Sets.	40
5.1	Difference Imaging Method.	41

CHAPTER I

INTRODUCTION

X-ray radiography can be used to non-destructively analyze features within an object. However, if the internal configuration of the object is not simple, the interpretation of the radiography projection data may present a problem. Because the bore of a solid rocket motor is very complex, computed tomography, (CT), is used to produce a transaxial slice image of the motor which represents a view perpendicular to the x-ray paths. Computed tomography is the best means of analyzing features within the rocket motor because the interpretation of the CT projection data presents no problem. By recording CT projection data during the test-firing of the motor, internal changes within the motor can be analyzed. This allows propellant burnout and propellant/case separation to be quickly identified and studied.

There are many ways to acquire computed tomography projection data from an object. A single source and detector can be used in computed tomography to scan a given object. To speed up the data acquisition process for a rocket motor, a single source and a curved bank of detectors are used to acquire a single fan-beam projection data set from the object instantaneously. Either the object or the data acquisition equipment can be rotated in order to acquire other projection data sets from the object. To accurately reconstruct the transaxial slice image, projection data sets must be acquired from the object at as many different projection angles as possible.

The transaxial slice image is estimated from the projection data sets by using a reconstruction algorithm. The transaxial slice image contains density information about the transaxial slice of the object from which the projection data sets

were acquired. The quality of the transaxial slice image increases as additional projection data sets are used to reconstruct the image.

Fan-beam projection data sets are normally acquired from the transaxial slice of the rocket motor during a test. The data acquisition equipment for the rocket motor is shown in Figure 1.1¹. The fan-beam data sets are acquired at evenly distributed projection angles.

Internal changes, as illustrated in Figure 1.2, can occur in the bore of the rocket motor during a test. The data sets required to reconstruct a given transaxial slice image of the rocket motor must be acquired simultaneously during the test in order to prevent edge smear in the reconstructed image. The data acquisition equipment can not be rotated around the motor fast enough to obtain projection data before an internal change occurs in the bore of the motor. Therefore, several sources and several banks of detectors are used to simultaneously record discrete projection data. Each of the reconstructed transaxial slice images is called a time point image and is used to analyze internal changes.

The amount of data acquisition equipment which can be used during a test is limited by the equipment cost and the space available around the motor. Therefore, only a small number of projection data sets can be used to reconstruct each time point image, and the quality of each image may be greatly degraded. As a consequence, regions of uniform density in the rocket motor are not uniform in the reconstructed time point image. Furthermore, boundaries between the regions are poorly resolved in the reconstructed time point image, and small anomalies will be unobservable.

The limited data problem has received considerable attention. Known image

¹ All figures and tables are located in the appendices.

information has been used as a priori information for limited data problems[1-13]². Two of the most commonly used methods which use known image information to reconstruct an image are the Radon transform method and the Fourier transform method. A Radon transform method has been used in the past to reconstruct an image from limited projection data[12]. A back-projection reconstruction algorithm was used with the Radon transform method. A Fourier transform method has also been used in the past to reconstruct an image from limited projection data[12]. A Fourier domain reconstruction algorithm was used with the Fourier transform method. The known image information used by the Radon and Fourier transform methods consisted of density and geometry information about the object. Other methods, which do not use known image information during reconstruction, have also been explored for the limited data problem[14-18]. Constrained optimization has been explored in the past for limited data problems[17]. However, none of these methods[1-18] used the conjugate gradient reconstruction algorithm. The conjugate gradient reconstruction algorithm was selected for the rocket motor problem since it has been shown to produce better quality images from rocket motor projection data than other reconstruction algorithms[19].

In this thesis, a correction-reconstruction process was developed to take advantage of known image information while using the conjugate gradient reconstruction algorithm. This information consists of the geometry and density acquired from a high quality pre-test CT image of the rocket motor. A large number of projection data sets can be easily and inexpensively acquired from the rocket motor before the test since they can be acquired consecutively.

Two images, a pre-test image and a first time point image, were reconstructed from a limited number of simulated parallel-beam projection data sets to test the

² The number located in brackets is the number of the source in the bibliography.

correction-reconstruction process. Model pre-test and first time point images were used to compute the simulated projection data. An error function was used to measure the quality of the reconstructed images. The error function value for a reconstructed image is the root mean square error between the model image and the reconstructed image. The quality of the pre-test and first time point images was studied after reconstructing both images with and without the use of a priori information. Both images were better, as shown by the error function values, when a priori information was used to reconstruct them.

Chapter II contains information about the conjugate gradient reconstruction algorithm which was used in the correction-reconstruction process. Chapter II also contains information about the two types of projection data used by the conjugate gradient reconstruction algorithm. Chapter III contains details of the correction-reconstruction process implemented for the rocket motor problem. Simulated noise-free projection data is used to test the correction-reconstruction process. The results from this experiment are located in Chapter IV. Chapter V contains a discussion of the results and recommendations for future work.

CHAPTER II

BACKGROUND INFORMATION

This chapter discusses the origin of the projection data used in this work and its use in reconstructing an image by using a conjugate gradient reconstruction technique.

1. TYPES OF PROJECTION DATA

Object Projection Data

An object projection data sample is acquired by passing an x-ray beam through the object[20]. An object projection path is shown in Figure 2.1. The object projection data sample is given by

$$p = -\ln(I/I_0) = \int_{-(0.5)L}^{+(0.5)L} u[x, y]dy. \quad (2.1)$$

The origin of the object domain is located at the center of the object. The value L is the length of the object projection path. The x-ray beam intensity I_0 is attenuated by the object to produce the beam intensity I . The relationship between the beam intensities and the attenuation function is called Beer's Law[20]. During data acquisition, a planar sheet of x-rays passes through the object. The plane of the object defined by this planar sheet is called the transaxial slice. Density information about the transaxial slice is obtained from the object projection data samples. The attenuation function $u[x, y]$ is the image which contains density information about the transaxial slice.

Detectors are used to collect and measure the x-ray beam intensities. A parallel-beam projection data set is acquired from the transaxial slice by using a straight bank of detectors and a distant source which produces nearly parallel

x-rays. A parallel-beam data set is shown in Figure 2.2. The projection angle, with respect to the coordinates x and y , of the parallel-beam projection data set is shown in Figure 2.2. A fan-beam projection data set is acquired from the transaxial slice by using a curved bank of detectors and a close source of x-rays. A fan-beam data set is shown in Figure 2.3. The projection angle, with respect to the coordinates x and y , of the fan-beam projection data set is shown in Figure 2.3.

A large number of projection data sets are normally acquired from the transaxial slice. The projection angles for the fan-beam projection data sets must be equally distributed from 0 to 360 degrees. However, the projection angles for the parallel-beam projection data sets need only be equally distributed from 0 to 180 degrees.

Image Projection Data

Strip integral and line integral projection data are two different types of image projection data. Strip integral image projection data is computed by the conjugate gradient reconstruction algorithm to produce an estimate of the attenuation function $u[x,y]$. Line integral image projection data is computed to simulate object projection data for testing the correction-reconstruction process in this work.

An image projection data sample is acquired by computing an integral through a model image, which simulates the transaxial slice of an object, with a finite number of pixels. An estimate image is computed from the image projection data. The grey level of the pixels in the model image represent attenuation values of the transaxial slice. The resolution of the model image is usually set to be greater than or equal to the resolution of the estimate image. The strip integral projection path and the line integral projection path, illustrated in Figure 2.4, are two different ways to compute an image projection data sample from a model image represented

in terms of individual pixel grey levels.

A strip integral image projection data sample is calculated by using effective pixel lengths. An effective pixel length is the area common to both a strip integral projection path and a pixel of the model image divided by the strip width. Effective pixel lengths are computed by using geometry parameters. A strip integral image projection data sample is given by

$$q_k = W^{-1} \sum_{m=1}^M a_{km} u_m. \quad (2.2)$$

The value a_{km} is the area common to both the k th strip integral projection path and the m th pixel of the model image, and the value M is the total number of pixels in the model image. The value u_m is the attenuation value of the m th pixel in the model image, and the value W is the width of the strip integral.

A line integral image projection data sample is calculated by making the width of the strip integral projection path very small. Only the pixel lengths are used to compute the data sample. A pixel length is the length of a line integral projection path through a pixel of the model image.

2. CONJUGATE GRADIENT RECONSTRUCTION ALGORITHM

An estimate of the attenuation function $u[x, y]$ can be reconstructed from projection data by using the conjugate gradient reconstruction algorithm. The conjugate gradient algorithm uses an iterative least squares technique, (ILST), to compute a correction factor which minimizes the weighted sum of the squared differences between object and strip integral image projection data[21]. This sum is referred to as a chi-square function value.

Chi-Square Function

The chi-square function value, the cost function used by the conjugate gradient algorithm, is given by

$$\chi^2(\underline{U}) = \sum_{k=1}^K (q_k - p_k)^2 h_k^{-2} = \underline{U}^T D \underline{U} - 2 \underline{E}^T \underline{U} + v \quad (2.3)$$

where

$$q_k = \sum_{m=1}^M g_{km} u_m. \quad (2.4)$$

The value q_k is the k th strip integral image projection data sample, and p_k is the value of the k th object projection data sample. The value h_k is the uncertainty with which the k th object projection data sample was measured. The uncertainty values are set to unity to reduce the memory requirement of the conjugate gradient algorithm[21].

The value K is the total number of object projection data samples. The value g_{km} is an effective pixel length, and the value u_m is the attenuation value of the m th pixel in the estimate image. The vector \underline{U} is the estimate image, and the value M is the total number of pixels in the estimate image. Each element of matrix D is given by

$$d_{ij} = \sum_{k=1}^K g_{ki} g_{kj} h_k^{-2} = \sum_{k=1}^K g_{ki} g_{kj}, \quad (2.5)$$

while vector \underline{E} is given by

$$e_i = \sum_{k=1}^K g_{ki} p_k h_k^{-2} = \sum_{k=1}^K g_{ki} p_k, \quad (2.6)$$

and the value v is given by

$$v = \sum_{k=1}^K p_k^2 h_k^{-2} = \sum_{k=1}^K p_k^2. \quad (2.7)$$

If K is greater than or equal to M , a non-iterative direct matrix inversion reconstruction algorithm can be used to reconstruct the estimate image from the object projection data. However, the direct matrix inversion algorithm can not be used to reconstruct the estimate image from limited projection data where K is less than M .

Iteration Scheme

The conjugate gradient algorithm is shown in Figure 2.5. The estimate image, for the n th iteration, is given by

$$\underline{U}_{n+1} = \underline{U}_n + f_n \underline{B}_n. \quad (2.8)$$

The vector \underline{U}_n is the initial solution for the n th iteration, and the vector $f_n \underline{B}_n$ is the correction factor computed during the n th iteration. The vector \underline{B}_n is the directional step, and the value f_n is the correction coefficient.

The correction coefficient is obtained by setting the derivative of $\chi^2(\underline{U}_{n+1})$, with respect to f_n , equal to zero[21], and the solution is given by

$$f_n = (\underline{B}_n^T \underline{C}_n) (\underline{B}_n^T D \underline{B}_n)^{-1} \quad (2.9)$$

where

$$\underline{C}_n = \underline{E} - D \underline{U}_n. \quad (2.10)$$

The directional step, \underline{B}_n , is chosen orthogonal to any previous directional steps[21], and it is given by

$$\underline{B}_n = \underline{C}_n - o_n \underline{B}_{n-1} \quad (2.11)$$

where

$$o_n = (\underline{C}_n^T D \underline{B}_{n-1}) (\underline{B}_{n-1}^T D \underline{B}_{n-1})^{-1}. \quad (2.12)$$

When $n = 0$, the vector \underline{B}_n is equal to the vector \underline{C}_n , and o_n is not needed. However, the vector \underline{U}_0 is not necessarily set to zero. Non-zero elements for vector \underline{U}_0 can be input into the conjugate gradient algorithm as the first initial solution. No specific termination criterion is available for the conjugate gradient algorithm. Such a criterion is needed to limit the number of conjugate gradient iterations necessary to reconstruct the estimate image.

CHAPTER III

CORRECTION-RECONSTRUCTION PROCESS

A priori information and object projection data are both used in the correction-reconstruction process, shown in Figure 3.1, to compute an estimate image of the rocket motor. This information consists of density and geometry information for the rocket motor. Known regions of the estimate image are corrected during each iteration of the process, and this image is then used as an initial solution by the conjugate gradient reconstruction algorithm. The correction of the known regions in the estimate image helps the conjugate gradient algorithm compute the unknown regions more accurately.

As shown in Figure 3.1, two types of iterations, conjugate gradient iterations and process iterations, are performed during the correction-reconstruction process. Conjugate gradient iterations are performed by the conjugate gradient reconstruction algorithm. The estimate image is not corrected in between conjugate gradient iterations. Process iterations are performed by the correction-reconstruction process. The estimate image is corrected in between process iterations. The correction-reconstruction process includes the conjugate gradient reconstruction algorithm as shown in Figure 3.1. A termination criterion is needed to determine the maximum number of conjugate gradient and process iterations necessary to reconstruct the estimate image. After the maximum number of process iterations is performed, the final estimate image is a time point image of the rocket motor.

1. CORRECTION OF KNOWN REGIONS

Sources of A Priori Information

Known regions of the estimate image are corrected on each iteration of the

correction-reconstruction process. The attenuation values in the known regions of the estimate image should be uniform in value. The location and extent of these regions are determined from a priori information about the estimate image. By correcting known regions of the estimate image, the unknown regions can be better computed from the available object projection data. A priori information about an estimate image can come from previously reconstructed time point images of the rocket motor since the time point images would be reconstructed in chronological order. A representative rocket motor time point image is illustrated in Figure 3.2.

A known region is one which has a uniformly distributed attenuation of given value. The unknown region contains the undetermined boundary between the propellant and background regions of the estimate image. The motor casing in the pre-test image is a known region of an estimate image because it remains unchanged in later time point images. The background region, outside the motor casing, of the pre-test image is also a known region because it remains unchanged in later time point images. The background region inside the motor casing of a time point image is called the bore region. The bore region of any previous time point image is a known region of an estimate image because it only gets bigger in later time point images due to propellant burnout.

A Priori Information Parameters

A priori information parameters are used to establish geometry and density information about known regions of the estimate image. Such a region is corrected by uniformly distributing an average attenuation value throughout that region. The average attenuation value can be established in two ways. It can be either given as an information parameter or computed from the attenuation values in the region. When negative attenuation values are computed by the reconstruction

algorithm, these negative attenuation values are set equal to zero on each iteration of the correction-reconstruction process. This density information can be used for any given reconstruction. The known regions for a rocket motor are shown in Figure 3.3.

As shown in Figure 3.3, the known annular motor casing, propellant, and background regions can be defined by geometric radii. These annular regions are centered in the middle of the estimate image and are used as known information parameters. The known circular background region in Figure 3.3 is defined by a single radius. The unknown annular region, containing the boundary between the bore and propellant regions, is also defined by radii.

2. TERMINATION CRITERION

Termination Values

Due to errors incurred by the conjugate gradient reconstruction algorithm, an excessive number of conjugate gradient or process iterations can degrade the estimate image during the process. Truncation error is suspected to be the source of error in the conjugate gradient algorithm. Upper limits for the number of conjugate gradient and process iterations must be established by the termination criterion for the conjugate gradient algorithm and the correction-reconstruction process. Therefore, two termination values are needed by the correction-reconstruction process to reconstruct a given time point image of the rocket motor. Data from test runs of the conjugate gradient algorithm and the correction-reconstruction process will be used to find these termination values.

The termination number of conjugate gradient iterations can be found by evaluating a termination function computed during a test run of the conjugate gradient algorithm. The termination number of process iterations can be found

similarly during a test run of the correction-reconstruction process. The termination function should be used to analyze any given reconstruction for the two required termination values. It was observed that computer time can be reduced by using the termination number of conjugate gradient iterations on each process iteration when a priori information is being used during reconstruction.

The chi-square function, computed by the conjugate gradient algorithm, could not be used as the termination function since it only involves projection data and can not clearly detect changes in the unknown region of the estimate image during the correction-reconstruction process. Thus, the difference function, which only involves image data, was used as the termination function for the process during a test run.

Difference Function Data

The difference function can be computed during a test run of either the conjugate gradient algorithm or the correction-reconstruction process. The difference function value is defined as the root mean square error between the estimate image and the first iteration estimate image in the unknown region, and it is given by

$$f_s = [I^{-1} \sum_{i=1}^I (u_i - s_i)^2]^{1/2}. \quad (3.1)$$

The value I is the total number of pixels in the unknown region, and u_i is the attenuation of the i th pixel in the unknown region of the estimate image. The value s_i is the attenuation of the i th pixel in the unknown region of the first iteration estimate image. The first iteration difference function value will always be zero.

The slope of the difference function, with respect to the iteration number, can be used to estimate the termination number of conjugate gradient or process

iterations required. The absolute value of the slope is examined for a percentage of the initial value of the slope. When the absolute value of the slope reaches this percentage of the initial value, the termination number of conjugate gradient or process iterations is assumed to have been reached. The value of one percent was arbitrarily selected for the termination criterion in Chapter IV.

The difference function, computed during a test run of the conjugate gradient algorithm, can be used to find the termination number of conjugate gradient iterations required. Likewise, the difference function, computed during a test run of the correction-reconstruction process, can be used to find the necessary number of process iterations. The termination number of conjugate gradient iterations would be used during the test run of the process to find the number of process iterations. An arbitrary number of iterations can be chosen for the length of a given test run. No a priori information would be used during the test run of the conjugate gradient algorithm to find the termination number of conjugate gradient iterations.

Difference function data can be used to analyze any given reconstruction for the required termination values. Several hundred time point images may be reconstructed from the rocket motor projection data to investigate the burnout of the propellant during the test-firing of the motor. It is not necessary to find the termination number of iterations for each and every time point image. A termination number of conjugate gradient iterations and a termination number of process iterations can be obtained from the analysis of the first time point image reconstruction. A termination number of conjugate gradient iterations and a termination number of process iterations can then be obtained from the analysis of the last time point image reconstruction. The higher termination number of conjugate gradient iterations and the higher termination number of process iterations would then be used to reconstruct all of the time point images.

CHAPTER IV

RESULTS OF THE PROCESS

1. METHOD OF TESTING THE PROCESS

Noise-free simulated projection data sets were used to demonstrate the performance of the correction-reconstruction process. To measure the quality of the estimate image during the reconstruction process, simulated projection data samples were computed from a model image of the rocket motor. The difference between the reconstructed image and the model image was used to measure the quality of the reconstructed image. Each region in the model image had a uniformly distributed attenuation value. The attenuation for the background regions was zero. The attenuation for the motor casing region was 200, and the attenuation for the propellant region was 100. Two different model images, one for pre-test conditions and one for the first time point image, were used to test the performance of the process.

Model Images

The model pretest image is shown in Figure 4.1. In practice, the pretest image is reconstructed from many projection data sets. Therefore, the reconstructed pretest image is a good source of density and geometry information. The model pretest image simulates the image of the motor before the test-firing where the bore of the rocket motor is usually small and symmetric.

The first time point image, shown in Figure 4.2, would be reconstructed from a small number of projection data sets. The bore of the rocket motor in the model first time point image is slightly larger than the bore in the model pretest image due to propellant burnout. Due to uneven burnout, the boundary between the bore

and propellant regions in the model first time point image is not as symmetrical as the boundary in the model pretest image. The boundaries of the bore regions in the model images consisted of sharp edges considered difficult to reconstruct. These sharp edges provided good tests of reconstructed image quality.

Use of Model Images

Error function values were used to measure the accuracy of the estimate image during reconstruction. The error function is defined as the root mean square error between the estimate image and the model image in the unknown region. The error function value is given by

$$f_m = [I^{-1} \sum_{i=1}^I (u_i - m_i)^2]^{1/2} \quad (4.1)$$

The value I is the total number of pixels in the unknown region, and u_i is the attenuation value of the i th pixel in the unknown region of the estimate image. The value m_i is the attenuation value of the i th pixel in the unknown region of the model image. The resolution of the model image and the estimate image was described on a 60 by 60 grid(3600 pixels).

Line integral image projection data, introduced in Chapter II, was used to simulate the rocket motor projection data. The image projection data was free of noise. A program which calculates fan-beam line integral image projection data sets was not available for use in testing the correction-reconstruction process. Since the type of geometry used to acquire the data sets does not make much difference during reconstruction, simulated parallel-beam projection data sets were used to test the correction-reconstruction process. The number of data samples in each set was 60. The image projection data were computed from the model pre-test and first time point images. The simulated projection data were then used, in place of object projection data, as input for the correction-reconstruction process.

2. RECONSTRUCTION OF THE IMAGES

The quality of the pre-test and first time point images was studied after reconstructing the images with and without the use of a priori information. The termination criterion, introduced in Chapter III, was used to find the number of conjugate gradient iterations and process iterations needed to obtain an acceptable reconstruction. Each test run required at least 20 iterations. A priori information is used to correct the estimate image during correction-reconstruction process iterations, and no a priori information is used to correct the estimate image during conjugate gradient reconstruction iterations.

Pre-test Image Reconstructions

The simulated pre-test projection data was acquired from the model pre-test image shown in Figure 4.1. The pre-test image is the zero time frame image. The pre-test image was reconstructed from equally distributed projection data sets. The projection angles of the parallel-beam data sets were equally distributed from 0 to 180 degrees. A priori information about negative attenuation values was used to correct the estimate image during the correction-reconstruction process. Negative attenuation values were set equal to zero in the estimate image on each process iteration. The unknown region covered the entire estimate image. Corrections of the negative attenuation values were made in the unknown region during the test run of the correction-reconstruction process.

The pre-test image was first reconstructed from 20 equally distributed data sets without the use of any a priori information during the test run of the conjugate gradient reconstruction algorithm. The information from this test run is contained in Table 4.1. Table 4.1 shows that the termination number of conjugate gradient iterations, including iteration zero, is five since the slope of the difference function

falls below one percent of the first slope after five iterations. The first 20 of the error function values plotted in Figure 4.3 are contained in Table 4.1. The error function values in Table 4.1 show that 11 iterations would have been a better choice for the termination number of conjugate gradient iterations since the error function value at 11 iterations is lower than the error function value at five iterations. The pre-test image, reconstructed from 11 conjugate gradient iterations and 20 data sets, is shown in Figures 4.4 and 4.5. The model bore boundary in Figure 4.1 is drawn, for comparison, in Figure 4.5. The image of Figure 4.5 contains only four different grey level values for the purpose of edge definition. Note that the boundaries of the motor casing in Figure 4.5 are not completely resolved.

The pre-test image was next reconstructed from 20 equally distributed data sets by using a priori information during the test run of the correction-reconstruction process. The information from this test run is listed in Table 4.2. Five conjugate gradient iterations were used during the test run of the process. Table 4.2 shows that the termination number of process iterations is 19 since the slope of the difference function falls below one percent of the first slope after 19 iterations. The error function values plotted in Figure 4.6 are contained in Table 4.2. The error function values in Table 4.2 show that 19 iterations is a good choice for the termination number of process iterations since the error function is minimum at 19 iterations. The pre-test image, reconstructed from 19 process iterations and 20 data sets, is shown in Figure 4.7. The model bore boundary in Figure 4.1 is drawn, for comparison, in Figure 4.7. The image of Figure 4.7 contains only four different grey level values for the purpose of edge definition. The reconstructed image of Figure 4.7 is better than that of Figure 4.5 as indicated comparing by the error function values of these images. The error function value of the image in Figure 4.7 is 14.12, and the error function value of the image in Figure 4.5 is 17.83. Thus,

a priori information reduced the error function value by about 21 percent.

To show how the quality of the estimate image improves with more projection data, seven pre-test images were reconstructed without the use of any a priori information. Each image was reconstructed using 11 conjugate gradient iterations. However, each image was reconstructed from a different number of equally distributed projection data sets. The seven images were reconstructed from 20, 24, 28, 32, 36, 40, and 44 data sets with evenly distributed projection angles. The error function values for the reconstructed images are plotted in Figure 4.8. Table 4.3 contains the values plotted in Figure 4.8. The increase of the error function value at 36 data sets is due to the projection angles of the data sets. Some information about the rocket motor is not in the projection data due to the particular angles of the 36 data sets. The error function value of the image at the 19th process iteration in Figure 4.6, where 20 data sets were used with a priori information, is less than the error function value of the image at 44 data sets in Figure 4.8, where no a priori information was used. Comparing the error function values, plotted in Figure 4.6 and Figure 4.8, shows that the use of a priori information has approximately the same effect on the pre-test image as doubling the number of projection data sets used to reconstruct the image.

First Time Point Image Reconstructions

The simulated first time point projection data was acquired from the model first time point image shown in Figure 4.2. The first time point image was reconstructed from equally distributed projection data sets. The projection angles of the parallel-beam data sets were equally distributed from 0 to 180 degrees. A priori information about the motor casing and background was used to reconstruct the first time point image during the correction-reconstruction process. This

geometry and density information was obtained from the pre-test image. An annular motor casing region and an annular background region were corrected in the estimate image on each process iteration. The annular background region was located outside the motor casing. Average attenuation values of the background and motor casing regions were given as known information parameters to correct the estimate image on each process iteration. The unknown region was circular and covered the bore and propellant regions inside the motor casing of the estimate image. Corrections were not made in the unknown region during the test run of the correction-reconstruction process.

The first time point image was reconstructed from five equally distributed data sets without the use of any a priori information during the test run of the conjugate gradient reconstruction algorithm. The information from this test run is contained in Table 4.4. Table 4.4 shows that the termination number of conjugate gradient iterations, including iteration zero, is four since the slope of the difference function falls below one percent of the first slope after four iterations. The first 20 of the error function values plotted in Figure 4.9 are shown in Table 4.4. The error function values in Table 4.4 show that four iterations is a good choice for the termination number of conjugate gradient iterations since the error function is minimum at four iterations. The first time point image, reconstructed from four conjugate gradient iterations and five data sets, is shown in Figure 4.10. The model bore boundary in Figure 4.2 is drawn, for comparison, in Figure 4.10. The image of Figure 4.10 contains only four different grey level values for the purpose of edge definition. The boundary between the propellant and bore in Figure 4.10 is very poorly resolved.

The first time point image was also reconstructed from five equally distributed data sets by using a priori information during a test run of the correction-reconstruction

process. The information from this test run is contained in Table 4.5. Four conjugate gradient iterations were used during the test run of the process. Table 4.5 shows that the termination number of process iterations is 11 since the slope of the difference function falls below one percent of the first slope after 11 iterations. The error function values plotted in Figure 4.11 are contained in Table 4.5. The error function values in Table 4.5 also show that 11 iterations is a good choice for the termination number of process iterations since the error function is minimum at 11 iterations. The first time point image, reconstructed from 11 process iterations and five data sets, appears in Figure 4.12. The model bore boundary in Figure 4.2 is drawn, for comparison, in Figure 4.12. The image of Figure 4.12 contains only four different grey level values for the purpose of edge definition. The boundary between the propellant and bore can be seen to be better resolved in Figure 4.12 than in Figure 4.10 as indicated by comparing the error function values of these images. The error function value of the image in Figure 4.12 is 18.97, and the error function value of the image in Figure 4.10 is 22.98. Thus, a priori information reduced the error function value by over 17 percent.

To show how the quality of the estimate image improves with more projection data, seven first time point images were reconstructed without the use of any a priori information. Each image was reconstructed using four conjugate gradient iterations. However, each image was reconstructed from a different number of equally distributed data sets. The seven images were reconstructed from five, six, seven, eight, nine, ten, and eleven data sets with evenly distributed projection angles. The error function values for the reconstructed images are plotted in Figure 4.13. Table 4.6 contains the the values plotted in Figure 4.17. The increase of the error function value at 7 data sets and 11 data sets is due to the projection angles of the data sets. Some information about the rocket motor is not in the projection

data due to the particular angles of the 7 data sets and the 11 data sets. The error function value of the image at the 11th process iteration in Figure 4.11 is less than the error function value of the image at 9 data sets in Figure 4.13. Comparing the error function values, plotted in Figure 4.11 and Figure 4.13, shows that the use of a priori information has approximately the same effect on the first time point image as doubling the number of projection data sets used to reconstruct the image.

CHAPTER V

SUMMARY

1. DISCUSSION OF THE RESULTS

The reconstructions in Chapter IV show that the quality of both images, the pre-test image and the first time point image, was better when a priori information was used to reconstruct them. The error function value of the reconstructed pre-test image decreased by 21 percent when a priori information was used to reconstruct the image. The quality of the motor casing boundaries in the reconstructed pre-test image was improved by correcting negative attenuation values during the correction-reconstruction process. The error function value of the reconstructed first time point image decreased by 17 percent when a priori information was used to reconstruct the image. The quality of the bore boundary in the reconstructed first time point image was improved by correcting the motor casing and background outside the motor casing during the correction-reconstruction process. Furthermore, the reconstructions in Chapter IV show that the use of a priori information has about the same effect on the pre-test and first time point images as doubling the number of projection data sets used to reconstruct the images.

By using known image information, the correction-reconstruction process reconstructs images better than the conjugate gradient reconstruction algorithm alone. The error function values in Chapter IV were computed by using model images of the rocket motor. Since model images are not available when object projection data is being reconstructed, difference function values must be used in the termination criterion for the correction-reconstruction process. The error function values in Chapter IV show that one percent of the initial value for the slope of the difference function is a good choice for the termination criterion.

2. SUGGESTIONS FOR FUTURE WORK

The difference function, used for the termination criterion, can be used to analyze the reconstruction of images from object projection data. However, the effect of noisy projection data on the correction-reconstruction process should be investigated. The error function can be used to measure the quality of images reconstructed from simulated projection data corrupted with noise.

The difference imaging method, shown in Figure 5.1, could be used with the correction-reconstruction process to possibly further improve the quality of the reconstructed time point image[13]. The difference image \underline{A}_3 contains only unknown regions of image \underline{A}_1 , and the a priori information image \underline{A}_2 contains only known regions of image \underline{A}_1 . The correction-reconstruction process can be used to better reconstruct the difference image \underline{A}_3 from the difference projection data \underline{P}_3 . The same a priori information that is used for the correction-reconstruction process can be used for the difference imaging method.

BIBLIOGRAPHY

BIBLIOGRAPHY

1. Baba, N., et al., "Iterative Relaxation Techniques for Image Reconstruction from Limited-Angle Projections", Optik, Vol. 68, No. 4, pp. 335-340, 1984.
2. Frieden, R. and Zoltani, C.K., "Maximum Bounded Entropy: Application to Tomographic Reconstruction", Applied Optics, Vol. 24, No. 2, pp. 201-207, January 1985.
3. Rangayyan, R., et al., "Algorithms for Limited-View Computed Tomography: An Annotated Bibliography and a Challenge", Applied Optics, Vol. 24, No. 23, pp. 4000-4012, December 1985.
4. Nassi, M., et al., "Iterative Reconstruction-Reprojection: For Limited Data Cardiac-Computed Tomography", IEEE Trans. on Biomedical Engineering, Vol. BME-29, No. 5, pp. 333-340, May 1982.
5. Tam, K.C. and Perez-Mendez, V., "Limits to Image Reconstruction from Restricted Angular Input", IEEE Trans. on Nuclear Science, Vol. NS-28, No. 1, pp. 179-183, February 1981.
6. Gordon, R. and Rangayyan, R.M., "Geometric Deconvolution: A Meta-Algorithm for Limited View Computed Tomography", IEEE Trans. on Biomedical Engineering, Vol. BME-30, No. 12, pp. 806-810, December 1983.
7. Tam, K.C., "Multispectral Limited-Angle Image Reconstruction", IEEE Trans. on Nuclear Science, Vol. NS-30, No. 1, pp. 697-700, February 1983.
8. Soumekh, M., "Image Reconstruction Techniques in Tomographic Imaging Systems", IEEE Trans. on Acoustics, Speech, and Signal Processing, Vol. ASSP-34, No. 4, pp. 952-962, August 1986.
9. Medoff, B.P., et al., "Image Reconstruction from Limited Data", IEEE, International Workshop on Physics and Engineering in Medical Imaging, pp. 188-192, 1982.
10. Medoff, B.P., et al., "Iterative Convolution Backprojection Algorithms for Image Reconstruction from Limited Data", J. Opt. Soc. Am., Vol. 73, No. 11, pp. 1493-1499, November 1983.
11. Sato, T., et al., "Tomographic Image Reconstruction from Limited Projections Using Iterative Revisions in Image and Transform Spaces", Applied Optics, Vol. 20, No. 3, pp. 395-399, February 1981.
12. Tam, K. and Perez-Mendez, V., "Limited-Angle 3-D Reconstruction Using Fourier Transform Iterations and Radon Transform Iterations", SPIE, 1980 International Optical Computing Conference, Vol. 231, pp. 142-148, 1980.
13. Heffernan, P.B. and Robb, R.A., "Difference Image Reconstruction from a Few Projections for Nondestructive Materials Inspection", Applied Optics, Vol. 24, No. 23, pp. 4105-4109, December 1985.
14. Rowan, W.H., et al., "Algorithms for Limited-Angle Computed Tomography", IEEE, International Workshop on Physics and Engineering in Medical Imag-

- ing, pp. 169-177, 1982.
15. Grunbaum, F.A., "A Study of Fourier Space Methods for Limited Angle Image Reconstruction", Numer. Funct. anal. and Optimiz., Vol. 2, No. 1, pp. 31-42, February 1980.
 16. Inouye, T., "Image Reconstruction with Limited Angle Projection Data", IEEE Trans. on Nuclear Science, Vol. NS-26, No. 2, pp. 2666-2669, April 1979.
 17. Katsulai, H. and Arimizu, N., "Reconstruction from Limited Angular Projection Data Using Constrained Optimization", IEEE Trans. on Nuclear Science, Vol. NS-20, No. 3, pp. 1870-1878, June 1983.
 18. Garden, K.L. and Robb, R.A., "3-D Reconstruction of the Heart from Few Projections: A Practical Implementation of the McKinnon-Bates Algorithm", IEEE Trans. on Medical Imaging, Vol. MI-5, No. 4, pp. 233-239, December 1986.
 19. Azevedo, S.G., et al., "Model-Based Algorithms for Limited-Data Tomography", Topical Proceedings of Industrial Computerized Tomography, pp.102-107, July 1989.
 20. Barrett, H.H. and Swindell W., Radiological Imaging, Academic Press, Vol. 2, pp. 375-464, 1981.
 21. Huesman, R.H., et al., Donner Algorithms for Reconstruction Tomography, University of California, pp. 29-34, October 1977.

APPENDICES

APPENDIX A

[FIGURES]

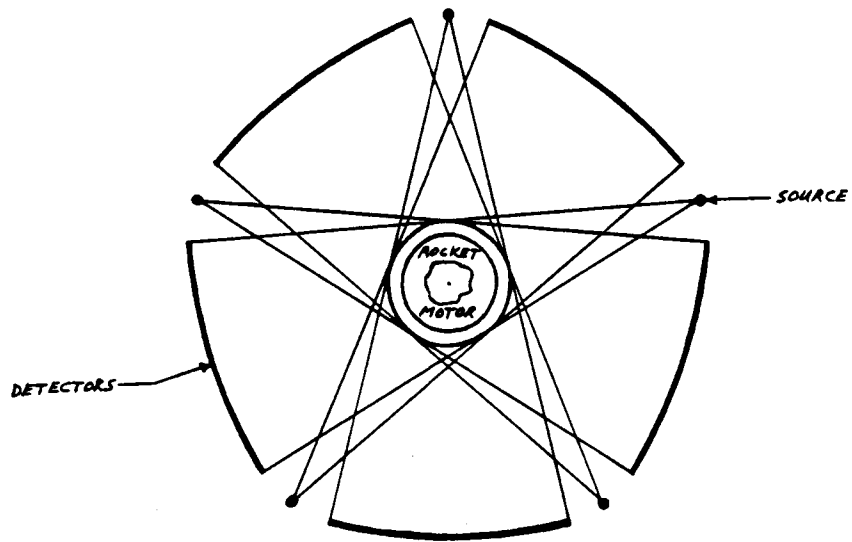


Figure 1.1. Data acquisition equipment.

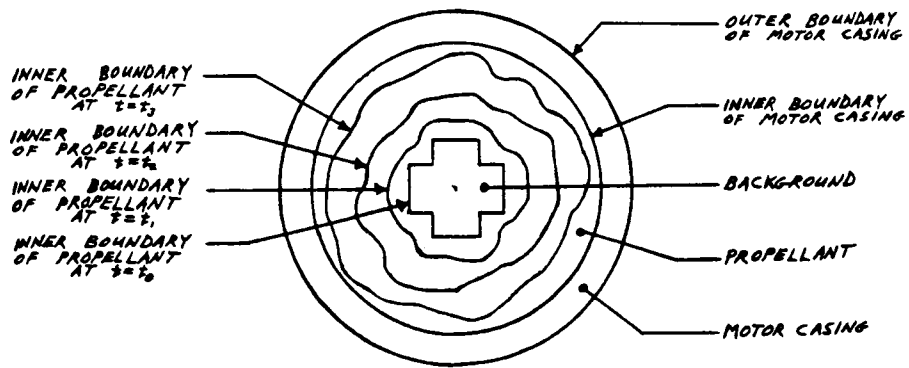


Figure 1.2. Burnout of propellant during test.

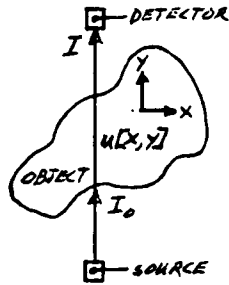


Figure 2.1. Object projection path.

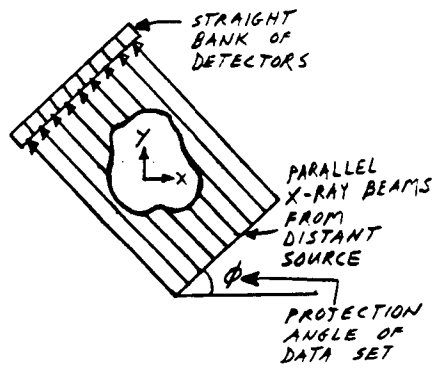


Figure 2.2. Parallel-beam data acquisition.

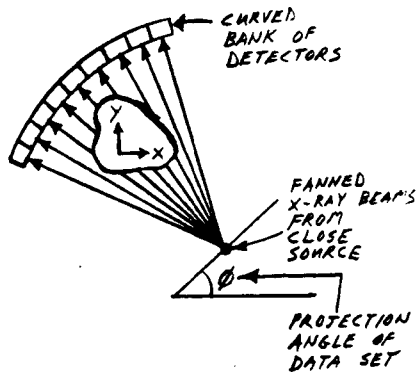


Figure 2.3. Fan-beam data acquisition.

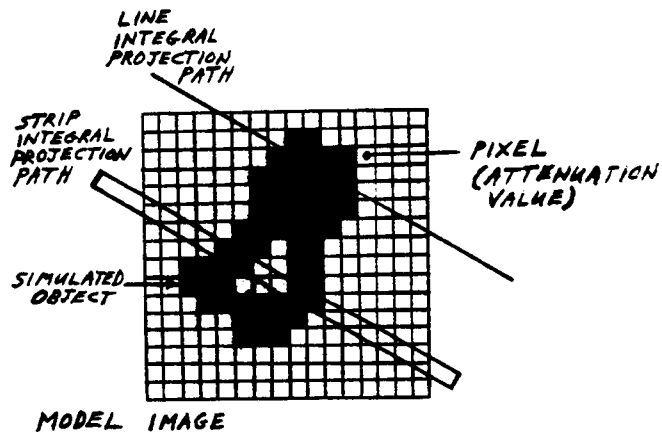


Figure 2.4. Image projection paths.

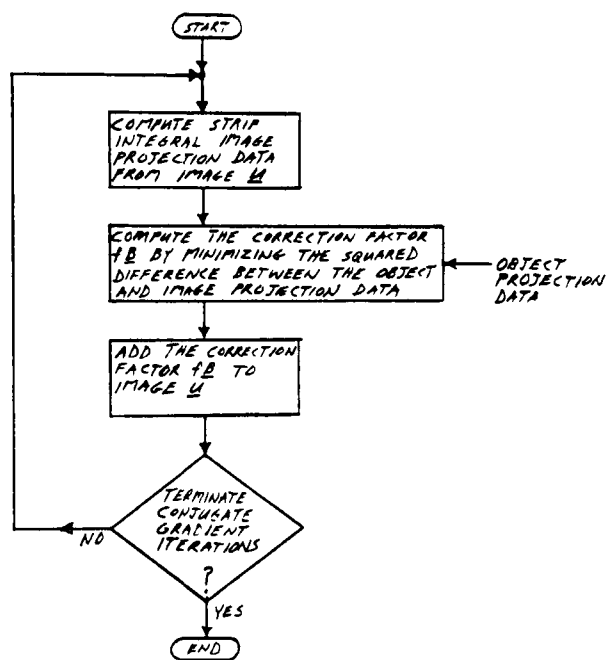


Figure 2.5. Conjugate gradient reconstruction algorithm.

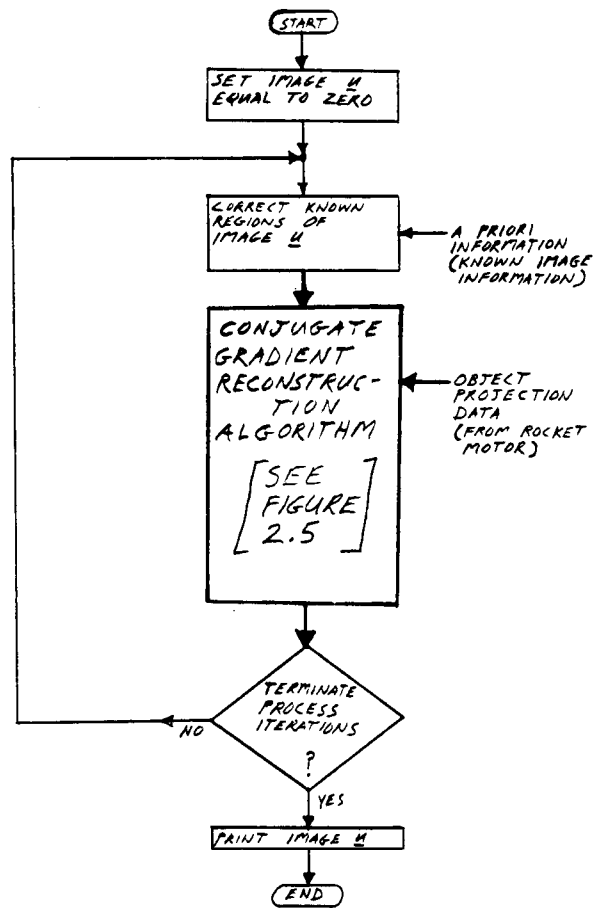


Figure 3.1. Correction-reconstruction process.

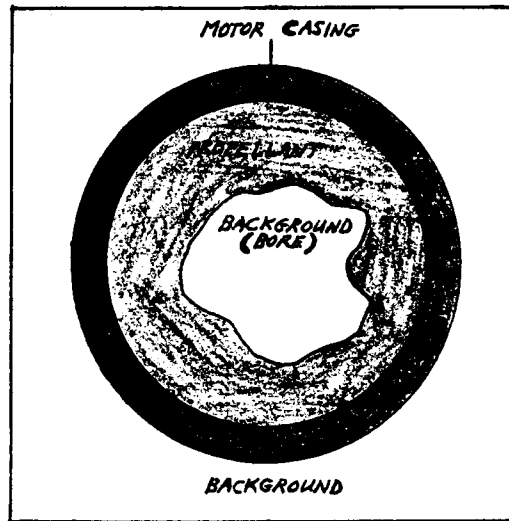


Figure 3.2. Rocket motor time point image.

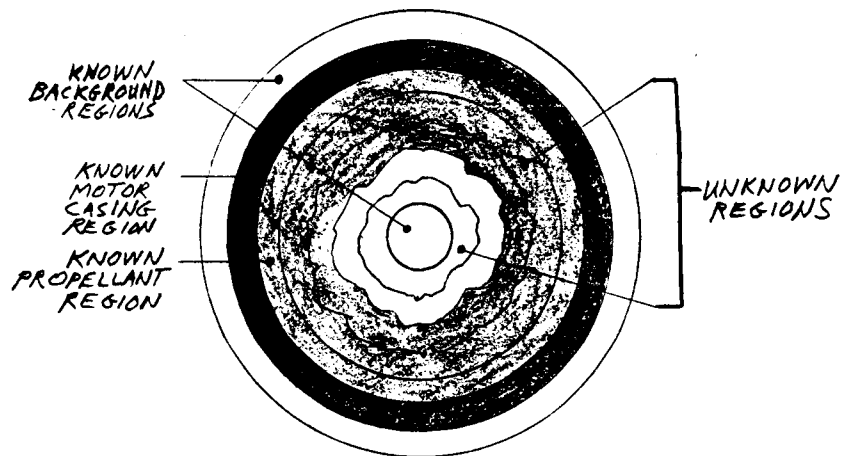


Figure 3.3. Known regions of estimate image.

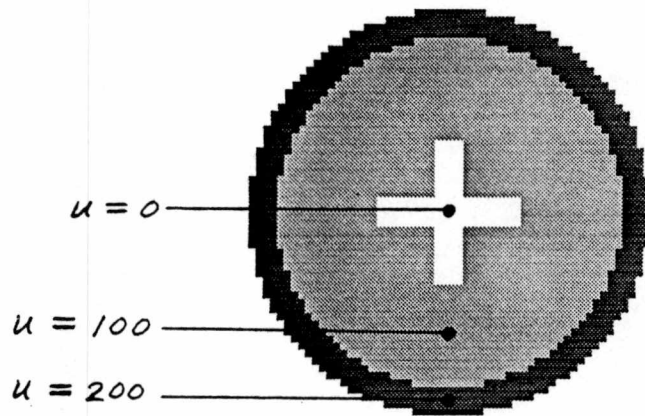


Figure 4.1. Model pre-test image.

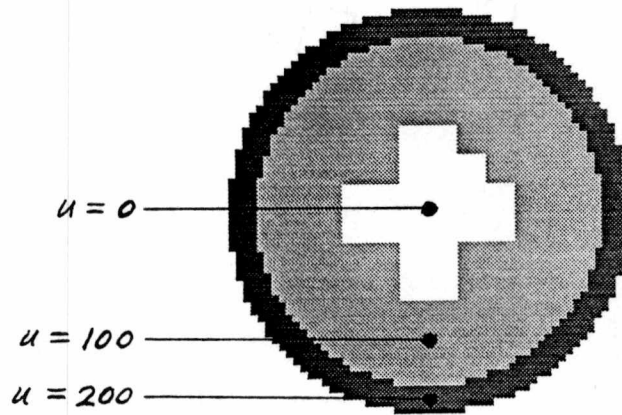


Figure 4.2. Model first time point image.

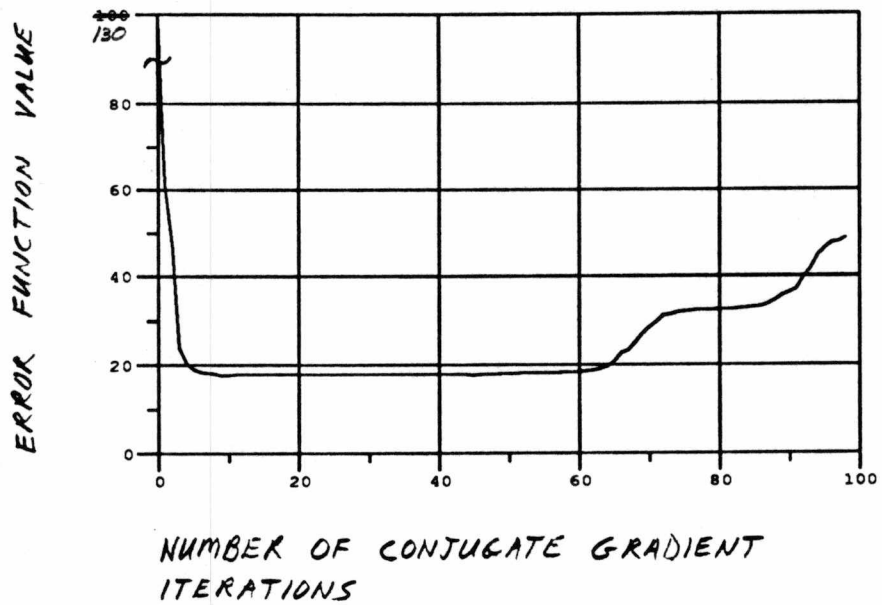


Figure 4.3. Error function values for conjugate gradient iterations of pre-test image reconstruction.

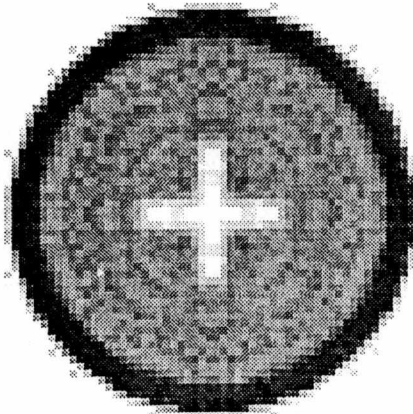


Figure 4.4. Pre-test image reconstructed from 11 conjugate gradient iterations(256 grey level values).

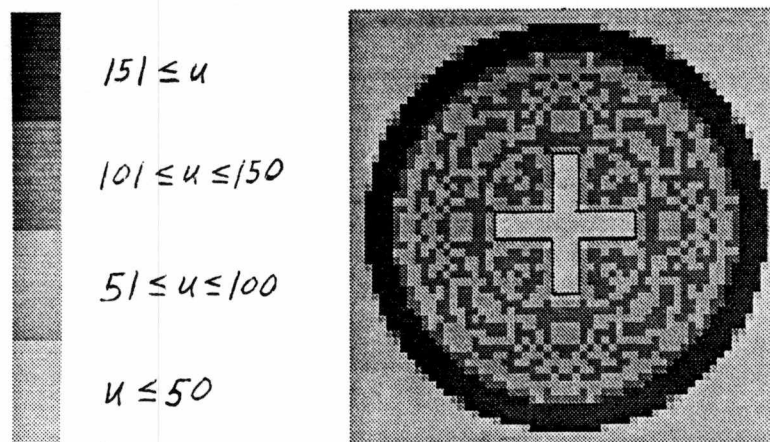


Figure 4.5. Pre-test image reconstructed from 11 conjugate gradient iterations(4 grey level values).

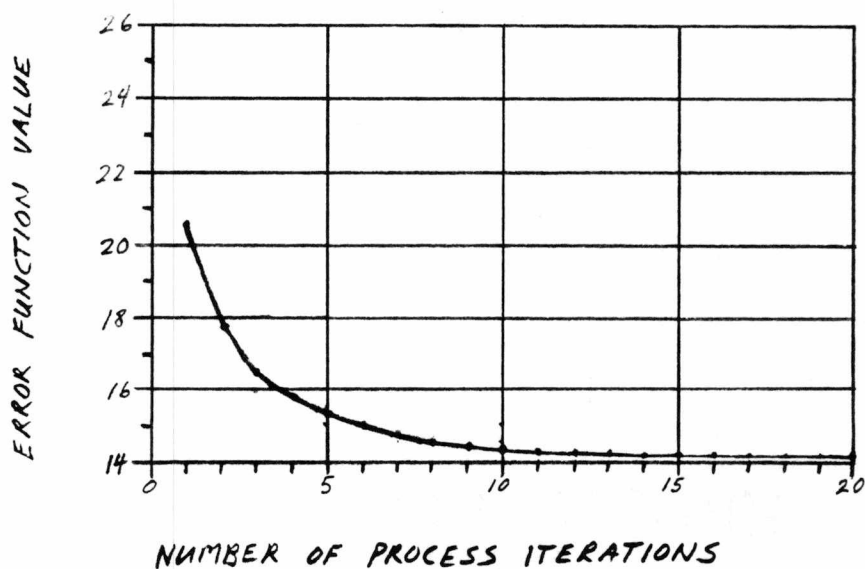


Figure 4.6. Error function values for process iterations of pre-test image reconstruction.

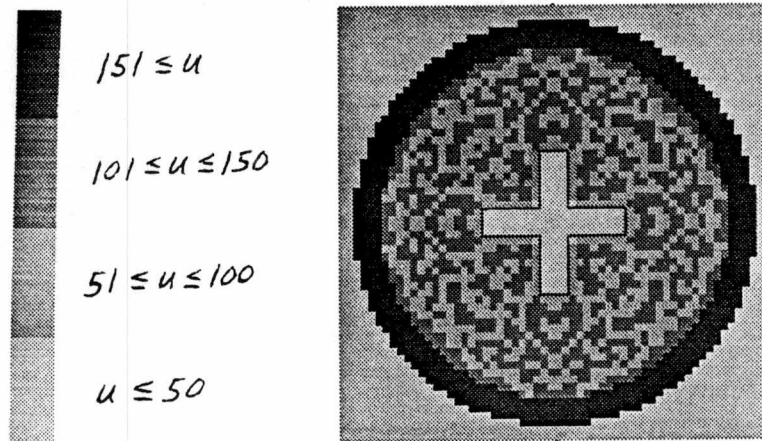


Figure 4.7. Pre-test image reconstructed from 19 process iterations(4 grey level values).

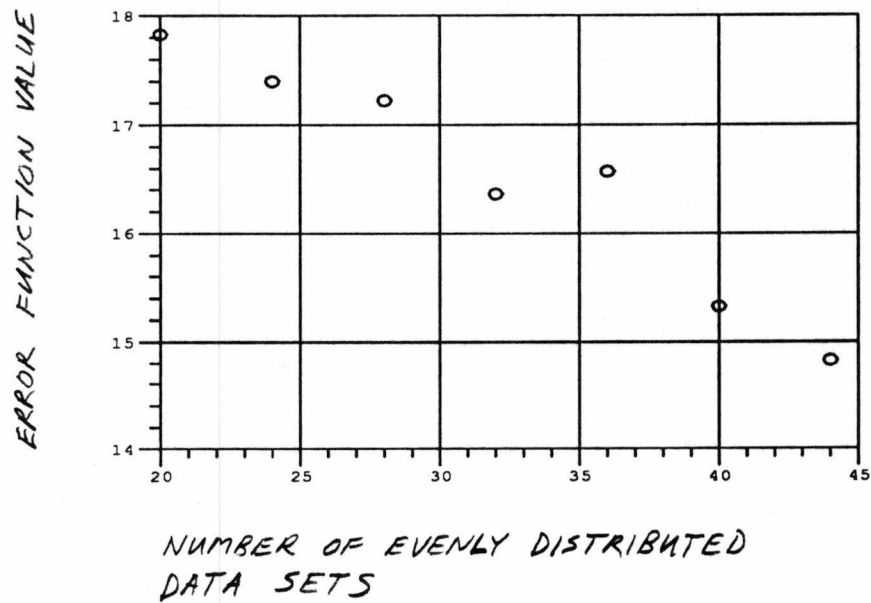


Figure 4.8. Error function values of pre-test images reconstructed from different numbers of data sets.

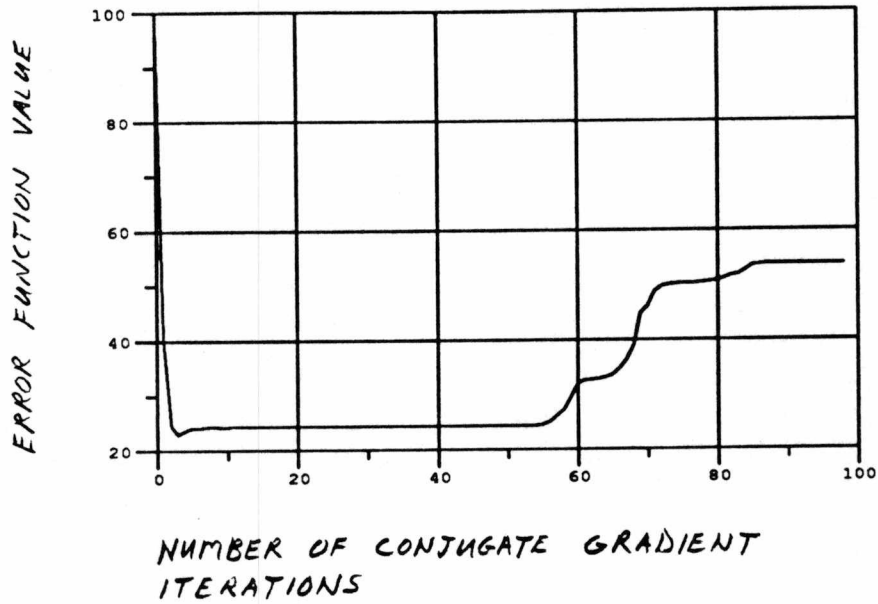


Figure 4.9. Error function values for conjugate gradient iterations of first time point image reconstruction.

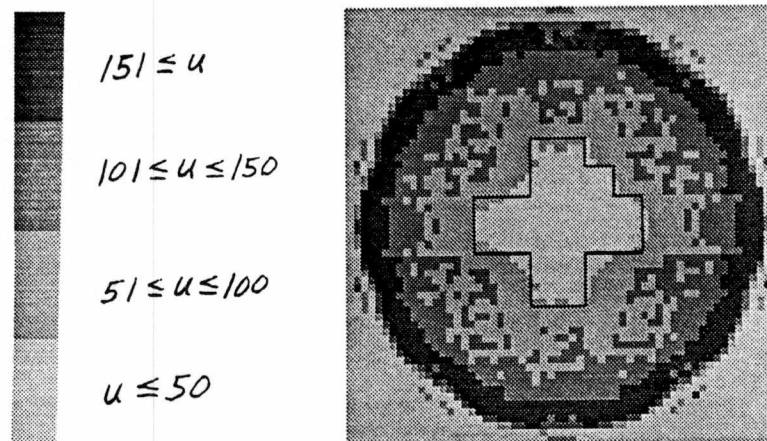


Figure 4.10. First time point image reconstructed from four conjugate gradient iterations(4 grey level values).

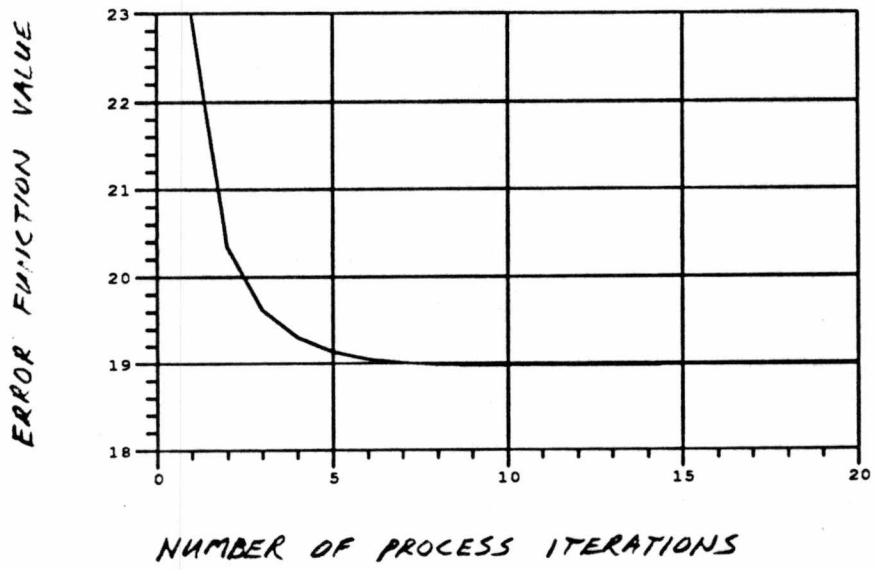


Figure 4.11. Error function values for process iterations of first time point image reconstruction.

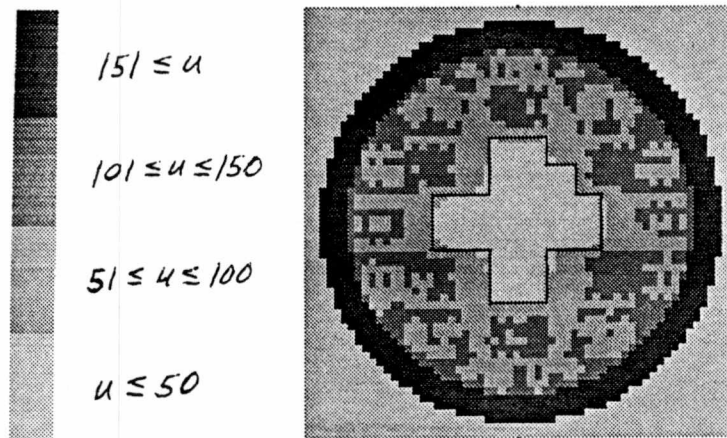


Figure 4.12. First time point image reconstructed from 11 process iterations(4 grey level values).

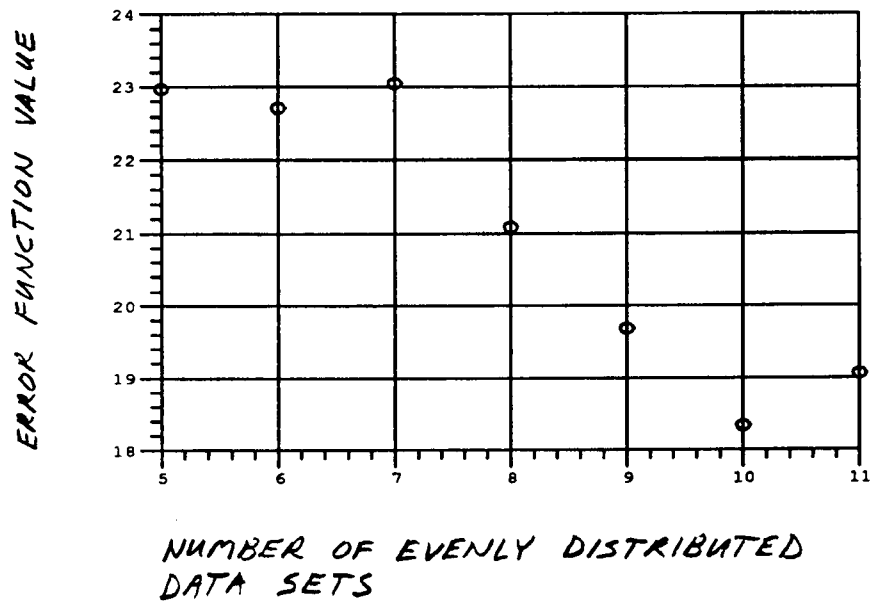


Figure 4.13. Error function values of first time point images reconstructed from different numbers of data sets.

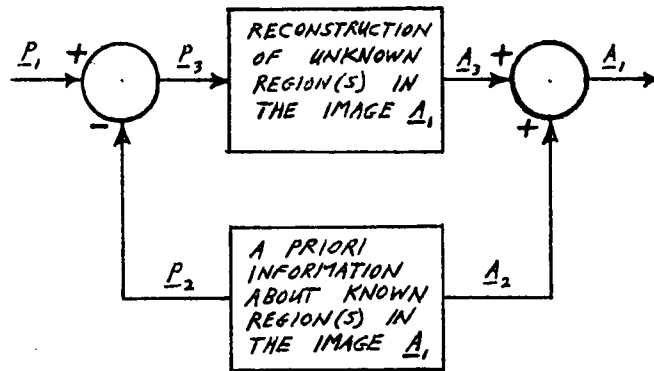


Figure 5.1. Difference imaging method.

APPENDIX B

[TABLES]

Table 4.1. Test run function values for conjugate gradient iterations of pre-test image reconstruction.

CONJUGATE GRADIENT ITERATION NUMBER	ERROR FUNCTION VALUE	DIFFERENCE FUNCTION VALUE	SLOPE OF DIFFERENCE FUNCTION
0	123.7669	0.000000	
1	61.46000	104.7255	104.7255
2	TERMI- 46.77705	111.1684	6.442902
3	NATION 24.04339	120.1037	8.935295
4	<-NUMBER 20.51447	122.0705	1.966805
5	19.19869	122.8263	0.7557983
6	18.52738	122.9776	0.1512985
7	18.42568	123.3448	0.3672028
8	18.23071	123.3310	-1.3801575E-02
9	17.88875	123.6647	0.3337021
10	17.83227	123.8712	0.2064972
11	17.92456	124.1406	0.2694016
12	17.96524	124.2327	9.2094421E-02
13	18.00814	124.3621	0.1294022
14	18.00452	124.3179	-4.4197083E-02
15	18.00265	124.4286	0.1106949
16	18.00591	124.4308	2.2048950E-03
17	18.01121	124.4609	3.0097961E-02
18	18.01837	124.4731	1.2199402E-02
19	18.02479	124.4657	-7.4005127E-03
20	18.03266	124.4793	1.3603210E-02

Table 4.2. Test run function values for process iterations of pre-test image reconstruction.

PROCESS ITERATION NUMBER	ERROR FUNCTION VALUE	DIFFERENCE FUNCTION VALUE	SLOPE OF DIFFERENCE FUNCTION
1	20.51447	0.000000	
2	17.71019	9.914655	9.914655
3	16.49580	10.38953	0.4748755
4	15.84767	12.43501	2.045480
5	15.29042	13.39167	0.9566603
6	14.97980	14.38580	0.9941301
7	14.68622	14.95283	0.5670300
8	14.51734	15.60811	0.6552801
9	14.36464	16.11057	0.5024605
10	14.27787	16.61480	0.5042286
11	14.21116	17.00977	0.3949699
12	14.18080	17.35522	0.3454514
13	14.16464	17.65483	0.2996101
14	14.15577	17.87890	0.2240696
15	14.14307	18.02836	0.1494598
16	14.13292	18.15655	0.1281891
17	TERMI- 14.12423	18.27040	0.1138496
18	NATION 14.11854	18.37774	0.1073418
19	<-NUMBER 14.11561	18.47925	0.1015091
20	14.11612	18.57747	9.8220825E-02

Table 4.3. Error function values of pre-test images reconstructed from different numbers of data sets.

NUMBER OF EVENLY DISTRIBUTED DATA SETS	ERROR FUNCTION VALUE
20	17.83227
24	17.39574
28	17.22364
32	16.35946
36	16.56930
40	15.32828
44	14.83476

Table 4.4. Test run function values for conjugate gradient iterations of first time point image reconstruction.

CONJUGATE GRADIENT ITERATION NUMBER	ERROR FUNCTION VALUE	DIFFERENCE FUNCTION VALUE	SLOPE OF DIFFERENCE FUNCTION
0	90.20794	0.000000	
1	TERMI- 40.38321	100.9054	100.9054
2	NATION 24.46995	96.06784	-4.837563
3	<-NUMBER 22.97619	93.33099	-2.736847
4	23.66388	93.20337	-0.1276245
5	24.13009	93.58323	0.3798599
6	24.17312	93.76156	0.1783295
7	24.29499	94.16952	0.4079590
8	24.37924	93.64214	-0.5273743
9	24.27186	93.49678	-0.1453629
10	24.29473	93.53520	3.8421631E-02
11	24.33944	93.57415	3.8948059E-02
12	24.35521	93.57419	3.8146973E-05
13	24.36168	93.59412	1.9927979E-02
14	24.35533	93.55804	-3.6079407E-02
15	24.35124	93.55487	-3.1661987E-03
16	24.34192	93.54919	-5.6838989E-03
17	24.33911	93.54748	-1.7089844E-03
18	24.33991	93.54637	-1.1062622E-03
19	24.33988	93.54723	8.6212158E-04
20	24.33740	93.53343	-1.3801575E-02

Table 4.5. Test run function values for process iterations of first time point image reconstruction.

PROCESS ITERATION NUMBER	ERROR FUNCTION VALUE	DIFFERENCE FUNCTION VALUE	SLOPE OF DIFFERENCE FUNCTION
1	22.97619	0.000000	
2	20.34071	7.186941	7.186941
3	19.62942	9.380466	2.193525
4	19.30980	10.52051	1.140043
5	19.14735	11.23295	0.7124405
6	19.06083	11.73241	0.4994602
7	19.01349	12.10255	0.3701391
8	18.99038	12.35220	0.2496500
9	18.97877	12.53486	0.1826601
10	TERMI- NATION 18.97505	12.66653	0.1316700
11	<-NUMBER 18.97466	12.75874	9.2210770E-02
12	18.97622	12.82802	6.9279671E-02
13	18.97831	12.87892	5.0899506E-02
14	18.98061	12.91788	3.8960457E-02
15	18.98272	12.94724	2.9359818E-02
16	18.98466	12.96997	2.2729874E-02
17	18.98636	12.98732	1.7350197E-02
18	18.98791	13.00094	1.3620377E-02
19	18.98929	13.01151	1.0569572E-02
20	18.99055	13.01995	8.4400177E-03

Table 4.6. Error function values of first time point images reconstructed from different numbers of data sets.

NUMBER OF EVENLY DISTRIBUTED DATA SETS	ERROR FUNCTION VALUE
5	22.97619
6	22.70660
7	23.04486
8	21.08400
9	19.68025
10	18.33521
11	19.05764

VITA

Alan Paul Smith was born in Biloxi, Mississippi on February 9, 1963. He attended elementary schools in Manchester, Tennessee and graduated from Manchester Central High School in May 1981. The following September, he entered the University of Tennessee at Knoxville. In August 1985, he received a Bachelor of Science degree in Electrical Engineering. The following September, he accepted a graduate research assistantship at the University of Tennessee Space Institute. In December 1991, he received a Master of Science degree in Electrical Engineering.